Influence of rotation on the (m,n)=(3,2) neoclassical tearing mode threshold in ASDEX Upgrade

S. Fietz, M. Maraschek, H. Zohm, M. Reich, L. Barrera, R. M. McDermott and the ASDEX Upgrade Team

Max Planck Institute for Plasma Physics, EURATOM Association , Garching, Germany

E-mail: sina.fietz@ipp.mpg.de

Abstract. The influence of rotation on the (m,n)=(3,2) neoclassical tearing mode onset and the marginal point at ASDEX Upgrade is investigated. In this context the different trigger mechanisms have been identified and the influence of not only the rotation but also the rotation gradient and the differential rotation between the resonant and the triggering surface on the NTM stability has been analysed. The existence of an upper NTM onset threshold can be observed in correlation with the rotation normalised to the Alfvén velocity. It can also clearly be verified that at ASDEX Upgrade the NTM onset threshold increases with co- and counter-current directed rotation and also with positive and negative rotation gradient.

Submitted to: *Plasma Phys. Control. Fusion*

1. Introduction

Neoclassical tearing modes (NTMs) are resistive MHD-instabilities. They are driven by a loss of helical bootstrap current which is caused by a flattening of the pressure profile across the magnetic island due to enhanced transport around the island. Once a seed island of sufficient size is generated this mechanism reinforces itself and the NTM grows. In present devices the occurrence of NTMs degrades the confinement and limits the maximal achievable β ($\frac{<p>}{B^2/2\mu_0}$). NTMs can decrease the plasma rotation and can even lead to disruptions in particular at low q_{95}. In large devices like ITER NTMs are likely to be performance limiting if they are not mitigated or avoided. To be able to control NTMs it is necessary to extrapolate the present understanding to larger devices with different conditions. A key parameter for the NTM physics and extrapolation is the rotation dependence. Compared to present devices, which typically have substantial rotation, ITER will be operated at low plasma rotation due to a low applied torque compared to the plasma inertia. With these differences the question arises how the NTM behaviour changes with rotation and if predictions can be made from present understanding. In addition to this, the general dependence of NTMs on different plasma parameters, especially the understanding of the seeding mechanism and the dependences at the NTM onset are an essential part for the control and avoidance of NTMs. Therefore, in the following, we want to address the question of how the plasma rotation influences the onset and the trigger process of NTMs. There exist several possibilities how plasma rotation can influence the NTM behaviour.

It has been proposed that changes in rotation or rotation shear can reduce the normally stabilising effect of the classical tearing stability index Δ' [1].

Rotation can also influence the stability of NTMs by means of small island effects. The ion polarisation current for example can be influenced by changes of the mode rotation in the plasma frame [2] [3].

A further important issue is the effect of rotation on the trigger mechanism. On one hand, the trigger instability itself can depend on plasma rotation as already found for the sawtooth instability [4] [5], on the other hand the seeding process due to magnetic coupling can be influenced by the differential rotation between the two resonant surfaces [6].

Finally, rotation can influence the island stability due to changes of the impact of error fields on the island or due to changes in the interaction between the island and the vessel wall. Changes in the island structure due to rotation are also possible.

Studies concerning the rotation dependence of NTMs have already been done at DIII-D [7], NSTX [8], JET[9] and other devices. At DIII-D experiments with co and counter injected beam torque were done. At NSTX only co-rotation data are available, which were obtained from experiments where the plasma rotation was varied via different co-injected beam torques and with an externally applied error field which acts as a drag on the plasma rotation. In both devices it was found that with decreasing co-rotation or rotation shear the NTM onset threshold decreases and that the role of

rotation shear on the NTM stability is more important than that of rotation alone. At DIII-D the NTM onset threshold decreases further with increasing counter-rotation. Similarly, for decreasing rotation shear, the onset threshold decreases continuously also when entering the region of negative shear, which is related to counter-rotation. This raised the question of whether a sign effect is responsible for the different behaviour with co- and counter-rotation or if the minimum onset threshold is shifted towards negative rotation which would indicate that an "offset" exists which is caused by diamagnetic drifts [1]. If this is the case, then it is possible that this minimum in rotation has not been reached yet at DIII-D and even stronger counter-current rotation data are needed to cross this minimum. Further, in[7] and [8] it was already shown that rotation has no influence on the ion polarisation current. Results from DIII-D and NSTX suggest that there exists an influence of rotation or rotation shear on the underlying tearing stability (Δ') which then is responsible for the rotation dependence of the NTM onset threshold [7] [1].
In the following we present the corresponding results from ASDEX Upgrade for the (3,2) NTM onset which differ in some respects from those at DIII-D and NSTX.

2. Definitions and experimental approach

The growth of an NTM can be described by the modified Rutherford equation [10] [11] for the island width W, with r_{res} the radius of the rational surface and $\tau_{\mathrm{res}} = \mu_0 r_{\mathrm{res}}^2/(1.22\eta)$ the resistive time-scale:

$$\begin{aligned}\frac{\tau_{\mathrm{res}}}{r_{\mathrm{res}}}\frac{dW}{dt} &= r_{\mathrm{res}}\Delta'(W) \\ &+ \frac{r_{\mathrm{res}}2\mu_0 L_{\mathrm{q}}}{B_{\mathrm{pol}}}\delta j_{\mathrm{BS}} a_{\mathrm{bs}}\left(\frac{W}{W^2+W_0^2}+\frac{W}{W^2+0.7w_{\mathrm{b}}^2}\right) \\ &- a_{\mathrm{pol}} r_{\mathrm{res}}\beta_{\mathrm{pol}}\left(\rho_{\theta\mathrm{i}}\frac{L_{\mathrm{q}}}{L_{\mathrm{p}}}\right)^2 g(\epsilon,\nu_{\mathrm{ii}})\frac{1}{W^3}\end{aligned} \tag{1}$$

The parameter $\epsilon = r_{\mathrm{res}}/R_0$ is the inverse aspect ratio at the resonant surface, $\rho_{\theta\mathrm{i}} = \sqrt{2m_{\mathrm{i}}k_{\mathrm{B}}T_{\mathrm{i}}}/eB_{\mathrm{pol}}$ is the ion poloidal gyro radius and β_{pol} is defined as $2\mu_0 p/B_{\mathrm{pol}}^2$ with p the total pressure and B_{pol} the flux surface averaged poloidal magnetic field strength at the resonant surface. The magnetic shear length is defined as $L_{\mathrm{q}} = q/q\prime$ whereas the gradient length of the pressure is $L_{\mathrm{p}} = -p/p\prime$ due to the normally negative pressure gradients. The coefficients a_{bs} and a_{pol} are of the order of unity.
Beside the classical tearing stability index Δ' in equation 1 the destabilising effect of the bootstrap current [12], [13] is included (second term on the right hand side). A simple and commonly used expression for the perturbation of the bootstrap current inside an island is $\delta j_{\mathrm{BS}} \approx -\epsilon^{\frac{1}{2}}\nabla p/B_{\mathrm{pol}}$ [14]. A more accurate one is given by the formula in [15]:

$$\delta j_{\mathrm{BS,Sauter}} = I(\psi)p_{\mathrm{e}}\frac{\left[(-0.5)\frac{p}{p_{\mathrm{e}}}\frac{\partial \ln p}{\partial\psi}+0.2\frac{\partial \ln T_{\mathrm{e}}}{\partial\psi}+(-0.25)\frac{\partial \ln T_{\mathrm{i}}}{\partial\psi}\right]}{\sqrt{<B^2>}} \tag{2}$$

with ψ the poloidal flux and $I(\psi) = RB_{tor}$, where R is the major radius and $B_{\rm tor}$ the toroidal magnetic field. The parameters p, $p_{\rm e}$, $T_{\rm e}$ and $T_{\rm i}$ present the total pressure, electron pressure and electron and ion temperature, respectively.

For an island size smaller than W_0 the destabilising effect of the bootstrap current is reduced due to a finite heat transport across the island which leads to incomplete pressure flattening inside the island [16]. For $W \sim w_{\rm b}$, which is often the case at the onset of NTMs, finite banana width effects have to be taken into account which additionally reduce the neoclassical drive [17] ($w_{\rm b}$ is the ion banana width).
In this context an NTM drive can be defined as $\mu_0 L_{\rm q} \delta j_{\rm BS}/B_{\rm pol}$ according to [8]. At ASDEX Upgrade the q profile measurements are insufficient to reliably detect changes in dq/dr. For this reason the dependences on $q(r)$ are not included in all following definitions (meaning $L_{\rm q}$=constant).
The third term in equation 1 corresponds to the ion polarisation current, which is also stabilising and important for small island widths [18]. This current is induced by the propagation of the island in the plasma frame. The ion polarisation current strongly depends on the ion collision frequency $\nu_{\rm ii}$ [19].
This dependence is included through the factor $g(\epsilon, \nu_{\rm ii})$ which is $\epsilon^{\frac{3}{2}}$ for 'collisionless' plasmas ($\nu_{\rm ii}/m\epsilon\omega_{\rm e}^*$ ¡¡1 and equal to 1 in the 'collisional' case ($\omega_{\rm e}^*$ is the electron diamagnetic drift frequency). In equation 1 the stabilising effects of toroidicity and shaping [20] and further small island effects are not taken into account. The stabilising small island effects are responsible for the need of a trigger mechanism which induces a seed island at the resonant surface. Except for the ion polarisation current, which is not responsible for the rotation dependence at the mode onset as already mentioned and discussed in [7] [1], no explicit rotation dependence is included in equation 1.
In the experimental analysis, we distinguish between different trigger mechanisms which, due to magnetic coupling, induce a seed island at the resonant surface. In figure 1 three example discharges are presented to illustrate the determination of the onset point and the corresponding seeding mechanisms for the following investigations. These (3,2) NTMs are triggered by a fishbone, a sawtooth and an ELM crash. Each onset point is clearly correlated with a distinct trigger mechanism. For most of the discharges the trigger mechanism could be identified unmistakably as either an ELM, a fishbone or a sawtooth crash. Cases, where the mode grows without any visible trigger, possibly destabilised by the $T_{\rm e}$ gradient, are also common. For some NTM onsets (1,1) activity was observed but the trigger mechanism could not be specified. In cases where at the mode onset multiple events took place the trigger mechanism is labelled as 'unclear'. For some islands also the marginal point could be determined. During the decay phase of stored energy and hence the β_{pol}, e.g. due to ramping down of the heating power, also the island width decreases. At the marginal point the island width evolution decouples from β_{pol} and decays away rapidly. This is illustrated for one special case in figure 2. For simplicity in this investigation we used the time evolution of the global $\beta_{\rm pol}$ and not the local one at the resonant surface like in all other analyses.

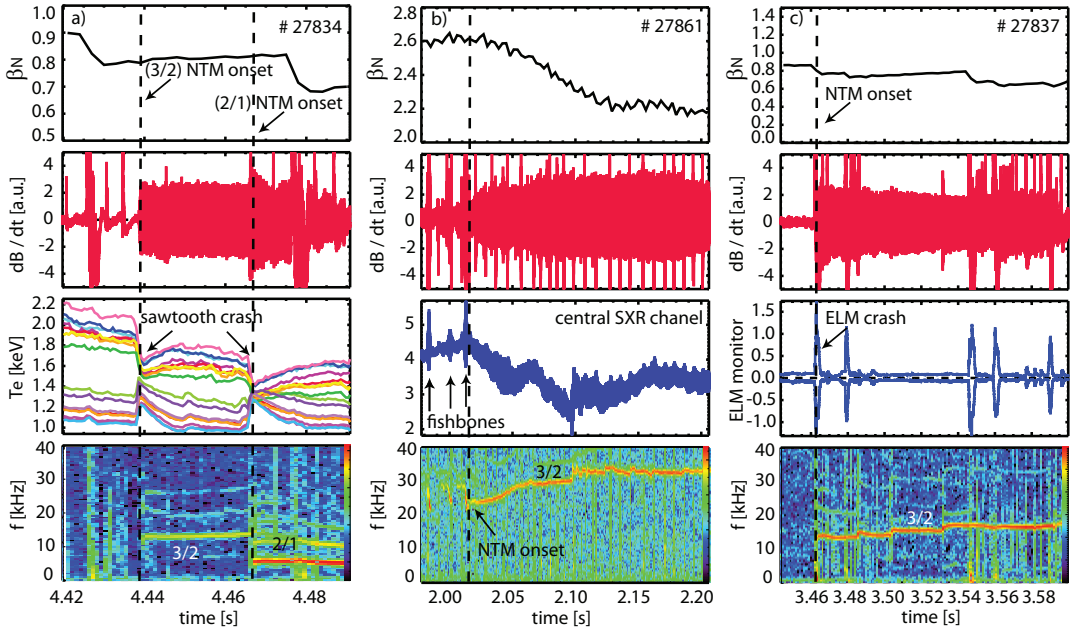

Figure 1. (3,2) Neoclassical tearing modes at ASDEX Upgrade triggered by a) a sawtooth crash b) a fishbone and c) an ELM with corresponding typical time-traces to illustrate the onset evaluation and trigger correlation

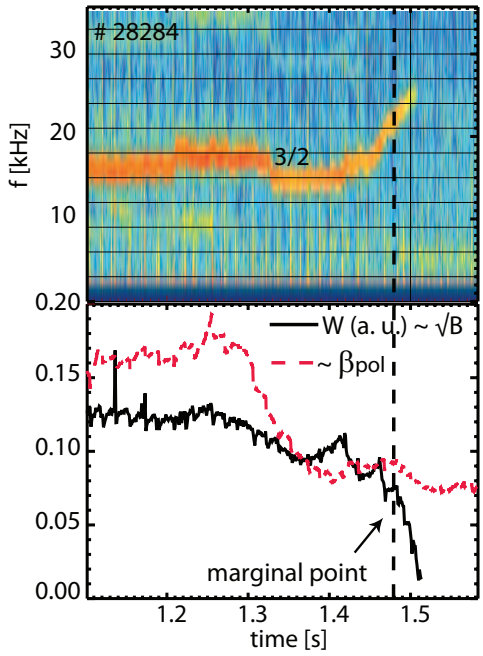

Figure 2. Illustration of the marginal point determination of a (3,2) Neoclassical tearing mode by the decoupling of the β_{pol} and the island width evolution

At ASDEX Upgrade the (m,n)=(3,2) NTM is the most common and hence a large data set of (3,2) NTM onset points with a wide range of plasma rotation is available. To extend the database, especially in the low rotation regime and with counter-rotation, dedicated experiments have been carried out. In these experiments the plasma rotation was varied by using different heating mixes. Two wave heating methods, ECRH (electron cyclotron resonance heating max. 4 MW) and ICRH (ion cyclotron resonance heating max. 6 MW) are available, neither of which apply a direct torque on the plasma. The torque input can be varied by using the neutral beam injection (NBI max. 20 MW) and combining radial and tangential beams. In normal operation the NBI is oriented in the co-direction relative to the plasma current. Experiments with counter-rotation can be done by reversing the plasma current and the magnetic field direction. With this the NBI is oriented in the counter-direction. The experiments with counter-rotation were limited in NBI heating power due to impurity influx created by first orbit losses. As a consequence the range of achievable counter-rotation was limited. For the following investigations all parameters are taken at the location of the magnetic island. The radial island location has been determined by using a soft X-ray diagnostic and a localisation method which is based on the correlation of the ECE channels (electron cyclotron emission) measuring the electron temperature T_e with a sampling rate of 1 MHz and the magnetic signals dB/dt [21]. The second method is very reliable and accurate and works satisfactorily for most of the discharges. The toroidal plasma rotation v_tor is measured via charge exchange recombination spectroscopy (CXRS) [22].

3. Experimental results

In this section the influence of the toroidal rotation velocity on the NTM onset threshold is investigated. A statistical analysis of all dependencies shown in this section is presented in table 1, where all the correlation coefficient are listed for comparison.
Similar to studies at other devices in the following, the rotation velocity is normalised to the Alfvén velocity ($v_\mathrm{A} = B_\mathrm{tor}/\sqrt{\mu_0 n_\mathrm{i} m_\mathrm{i}}$, with B_tor the toroidal magnetic field, n_i the ion density, m_i the ion mass and μ_0 the magnetic vacuum permeability), due to the only marginal dependence of the NTM onset threshold on toroidal rotation alone. This normalised quantity is then defined as Ma_A. In figure 3 the global β_N at the NTM onset is plotted against the normalised rotation. Here the β_N is defined as $\beta aB/I_\mathrm{p}$ with a the minor radius, I_p the plasma current and B the magnetic field. Also indicated is the hypothetical achievable parameter range in β_N and Ma_A (area below the machine limit), which is estimated assuming a momentum confinement time equal to the energy confinement time and an H_{98}-factor of one. In this calculation the plasma rotation was varied by including different mixtures of the heating methods (NBI max. 20 MW and wave heating max. 10 MW) available at ASDEX Upgrade. The calculated data points are shown as grey-blue boxes in figure 3 which indicate the hypothetical experimentally achievable data range. In figure 3 the β_N at the NTM onset linearly increases with increasing normalised plasma rotation for co- and counter-rotation. This is more distinct

for the co-current rotation data, which can also be seen from the correlation analysis presented in table 1, but however the a trend is also visible for counter-current rotation.

Additionally, it is clearly visible that the NTMs limit the maximal achievable beta and hence, limit the plasma operation below the machine limit. Since heating with NBI not only increases the β_{N} but also exerts a torque on the plasma and hence increases plasma rotation at the same time the fact that the machine limit is higher than the achievable β_{N} also indicates that this linear dependence of the β_{N} and the rotation velocity at the NTM onset is not trivial.
Considering that the NTM onset threshold can be described more accurately by the perturbation of the bootstrap current inside the island, which is proportional to $\beta_{\mathrm{pol}}/L_{\mathrm{p}}$, another analysis method using local parameters is shown in figure 4. In this plot additional data points from different discharges where no NTM is present are included. An upper NTM onset threshold is clearly visible in this analysis, which linearly increases with Ma_{A} in the region of high rotation. All of the data points, including the NTM onset data and the data without NTMs, are situated below this threshold in the metastable region. This means that plasma operation is ultimately limited by NTMs when this threshold is reached and that the region above this threshold cannot be realised in experiment. This is different when the resonant q-surface is not present or the NTM is actively stabilised. The lower NTM threshold, which defines the minimum required drive for the occurrence of an NTM and can in principle be explained by the Rutherford equation, seems not to depend on rotation. In the region of low normalised rotation (¡1 Ma_{A}), where the intersection of the upper and lower threshold should be, the upper threshold seems not to depend on rotation anymore. In this region of low rotation the discharges are mainly heated by wave heating, which seems to change the NTM stability behaviour or the trigger mechanisms and blurs the boundaries.

The scatter of the NTM onset data in the metastable region (green coloured area) is caused by the different trigger events. The trigger process is different for every NTM onset, even if the triggering instability is the same, and hence leads to different seed island sizes and in consequence different onset thresholds.

Although the counter-current rotation data is limited, also with this analysis method a trend towards increasing co- and counter-rotation with increasing NTM onset threshold is visible which leads to a minimum threshold in the region of zero rotation. For co-current rotation this trend can also be seen for all of the different trigger sub-sets (compare table 1). This disagrees with the experiments at DIII-D, where a further decrease of the onset threshold with counter rotation was found. As already mentioned in previous works it was suggested that an offset of the threshold minimum exists which was not reached at DIII-D [1]. According to [23] the correct parameter to investigate the dependence of the NTM threshold on rotation is the velocity of the island in the laboratory frame $f_{\mathrm{NTM,lab}}$, where the local radial electric field E_{r} is zero. Considering this corrected island rotation, an offset as observed at DIII-D, can be explained. This island rotation frequency in the laboratory frame is defined as $f_{\mathrm{NTM,lab}} = n f_{\mathrm{plasma,CXRS}} + f_{\mathrm{i}}^{\star}$, where $f_{\mathrm{i}}^{\star}$ is the flux surface averaged ion diamagnetic drift

frequency, defined as $nk_{\mathrm{B}}T_{\mathrm{i}}(dp_{\mathrm{i}}/d\psi)/ep_{\mathrm{i}}$ (n is the toroidal mode number) and $f_{\mathrm{plasma,CXRS}}$ is the plasma toroidal rotation frequency at the location of the island. As discussed in [1] this expression leads to a finite $f_{\mathrm{NTM,lab}}$ even if $f_{\mathrm{plasma,CXRS}}$ is zero and in consequence for $f_{\mathrm{NTM,lab}} = 0$ an offset in the counter direction at $f_{\mathrm{plasma,CXRS}} \approx f_{\mathrm{i}}^{\star}$ exists.
In figure 5 the mode frequency f_{NTM} at the onset is plotted against the toroidal plasma rotation frequency $f_{\mathrm{plasma,CXRS}}$ at the resonant surface at the time of the NTM onset. A linear regression fit is also indicated together with the corresponding standard deviation (grey shaded area). Referred to theory the difference of this fit and the assumption $f_{\mathrm{NTM}} = n \cdot f_{\mathrm{plasma,CXRS}}$ is due to the ion diamagnetic drift frequency. Since this difference is within the standard deviation, as can be seen in figure 5, the ion diamagnetic drift frequency is smaller than the error bars of our analysis. For the counter rotation points a small ion diamagnetic drift frequency could exist but due to to the small amount of data points here this observation is marginal and it is hard to draw any conclusion from this. So concluding from the observations of the co-current data the ion diamagnetic drift frequency is smaller than the uncertainties of the frequency measurements and we expect to have no obvious offset of the threshold minimum in figure 4. In any case the data show a clear linear dependence of the onset threshold with co- and counter-current rotation.
When plotting the NTM onset threshold against Ma_{A} it is noteworthy that in the region of low rotation NTMs are mostly triggered by a sawtooth crash or appear without any trigger. This can be seen in both figure 4 and figure 3. It is well known that a sawtooth crash can lead to a strong perturbation at the resonant surface and this results in a low NTM threshold. In contrast, based on the fact that the triggerless case is seen as the weakest trigger mechanism, one would expect these cases to have a higher onset threshold. From this discrepancy one can infer that there exists an influence of plasma rotation on the underlying tearing stability. This means that at lower plasma rotation the Δ' term changes such that the plasma is less stable against NTMs as already proposed in [7] and [1].
Further investigations have been made to disentangle the influence of rotation on the island stability itself as opposed to the trigger mechanism. To this end the NTM behaviour at the marginal point, where no influence of the trigger mechanism exists, has been analysed.

This dependence is shown in figure 6. The correlation analysis (table 1) reveals that only a very weak dependence of the NTM drive at the marginal point on the normalised rotation velocity exists but additionally this correlation is not significant, which rather implies that no dependence exists than the other way around. From this one can conclude that, so far, no dependence is observed at the marginal point, which could additionally indicate that the rotation dependence at the onset is caused by an impact of rotation on the trigger mechanism.

However, the scatter of the data makes it difficult to exclude a dependence on Δ', which would lead to a dependence at the marginal point and which can still be hidden in dependencies we have not included in our analysis.

All rotation dependencies have also been analysed using the formulae of Sauter to describe the NTM onset threshold, defining a 'bootstrap drive' as was done in [8] and [15] and using equation 2. With this expression the scatter in the scalings is increased and the quality of the correlation of the whole dataset, especially for co-current rotation, is reduced. This is different compared to results from other machines but can be explained due to a stronger weighting of the density profile in this expression for the 'bootstrap drive' which has, at least at ASDEX Upgrade, large uncertainties.
As discussed above, also differential rotation is a possible candidate to influence the NTM onset threshold, either simply the differential rotation at the resonant surface or the differential rotation between the trigger and the island surface. In figure 7 a linear dependence of the NTM onset threshold and the differential rotation (the rotation gradient) at the resonant surface is visible for the whole data set just as for most of the different trigger subsets. Compared to figure 4 the scatter of the data is a little bit increased which results in a smaller correlation coefficient (compare table 1).

At NSTX the correlation of the scaling is improved when using the rotation shear [8] compared to only the rotation gradient. Due to the absence of reliable q profile measurements it is not possible to prove this at ASDEX Upgrade.
In figure 8 the differential rotation between the island surface and the flux surface where the trigger is located is plotted against the NTM threshold. The cases in which ELMs were identified as trigger mechanisms, Δv_{tor} is calculated as the difference of the toroidal rotation velocity at the resonant surface and the toroidal rotation velocity at the pedestal top, whereas the difference of the velocity at the q=1 surface and the resonant surface is used when the trigger mechanism is defined as fishbone, sawtooth crash or any other mode activity at the q=1 surface. The NTM onset threshold increases with differential rotation for the ELM and fishbone triggered cases whereas no dependence on differential rotation is seen for the sawtooth triggered cases. This means that ELMs and fishbones can more easily lead to a sufficiently large perturbation at the resonant surface when the rotation profile is flat, whereas for sawtooth crashes the rotation profile seems to have no impact on the triggering mechanism. This is an indication that the magnetic reconnection forced by a sawtooth crash at the resonant surface is strong enough to induce a sufficiently large seed island independent of the rotation profile. This is also in line with the observation that NTMs triggered by a sawtooth crash can appear at a low onset threshold.

4. Conclusion

In this paper, the rotation dependence of (3,2) NTMs at ASDEX Upgrade has been analysed. The investigated data base includes around 70 discharges with co and counter rotation and different heating mixes. Additionally, the different trigger mechanisms at the NTM onset have been identified. These analyses show an increasing onset threshold with increasing (normalised) co and counter rotation. Compared to investigations at DIII-D where a further decrease of the onset threshold with counter rotation was found,

Table 1. Analysis of the statistical dependence of the NTM onset threshold on the normalised rotation at the NTM onset (figure 3 and 4) and the marginal point (figure 6), the normalised rotation gradient (figure 7) and the differential rotation (figure 8) at the NTM onset. Additionally the correlation parameter for the dependence of the NTM onset threshold on simply the rotation and for the dependence of the Ma_{A} on the onset threshold definition developed by Sauter (equation 2) is indicated. The correlation parameter R is shown for the whole data set in co and counter current direction. For some dependences also the correlation parameters for the different trigger sub-sets are shown. If there are too few data points, or the data range is too small, the correlation is not significant. This is indicated with an x. The abbreviation n.v.t. stands for "no visible trigger".

	co	counter	ELM	Fishbone	Sawtooth	n.v.t.	1/1
v_{tor} vs. β_{N}	0.47	-0.63	-	-	-	-	-
Ma_{A} vs. β_{N}	0.71	x	-	-	-	-	-
Ma_{A} vs. $\beta_{\mathrm{pol}}/L_{\mathrm{p}}$	0.60	-0.68	0.46	0.65	0.56	0.72	x
Ma_{A} vs. $\delta j_{\mathrm{BS,Sauter}}$	0.45	x	-	-	-	-	-
Ma_{A} vs. $\beta_{\mathrm{pol}}/L_{\mathrm{p}}$ (marginal)	x (0.13)	-	-	x	-	0.92	-
$(-dv_{\mathrm{tor}}/dr)/v_{\mathrm{A}}$ vs. $\beta_{\mathrm{pol}}/L_{\mathrm{p}}$	0.50	-0.7	x	0.58	0.56	0.46	x
$\Delta v_{\mathrm{tor}}(r_{\mathrm{res}}, r_{\mathrm{trigger}})/v_{\mathrm{A}}$ vs. $\beta_{\mathrm{pol}}/L_{\mathrm{p}}$	0.26	-	0.47	0.56	x	-	x

at ASDEX Upgrade the region of minimum onset threshold could be reached and the trend with counter rotation clearly verified. As a consequence the onset threshold increases with positive and negative rotation gradient as well. The analysis of the mode frequency indicates that at ASDEX Upgrade no offset of the threshold minimum towards negative rotation exist. This is due to a small ion diamagnetic drift frequency which is in the order of the uncertainties of the analyses. But nevertheless it is still possible that at DIII-D the ion diamagnetic drift is larger and an offset exist and the minimum has just not been reached yet. In consequence the results from DIII-D and AUG are not in fact contradictory. At ASDEX Upgrade a range of onset β-values is found where the upper limit scales linearly with rotation. This formation of an upper NTM threshold limits the plasma operation below the machine limit. In the region of low rotation the upper threshold no longer depends on rotation which indicates that in this region the NTM behaviour or the triggering process is different. At the marginal point no dependence of the NTM threshold on rotation is found. This leads to the assumption that the trigger mechanism depends on rotation which then leads to a rotation dependence at the NTM onset. On the other hand from the scattered data it is hard to conclude that no influence of rotation on the equilibrium stability index (Δ') exists. It is still possible that this influence is hidden in dependencies we have not taken into account in our analysis. Additionally the observation of NTMs without any trigger appearing at a low NTM threshold and low rotation reveals that the underlying Δ' is less negative (stabilising) at low rotation. Further we identified that in contrast to the ELM and fishbone triggered cases the triggering of an NTM via a sawtooth crash is independent of the rotation profile and can therefore occur also at low onset threshold. This leads to the assumption that the perturbation at the resonant surface induced by a sawtooth

crash is always strong or that the trigger mechanism differs from the others.
For ITER, which will be operated at low rotation, the results presented in this work also reveal a low beta limit due to NTMs. The analysis reveals that in the range of low rotation the appearance of NTMs is possible even at low β-values. From this point of view it will be crucial to further investigate the NTM parameter dependencies in order to learn how best to avoid NTMs in ITER such that the desired performance can be attained.

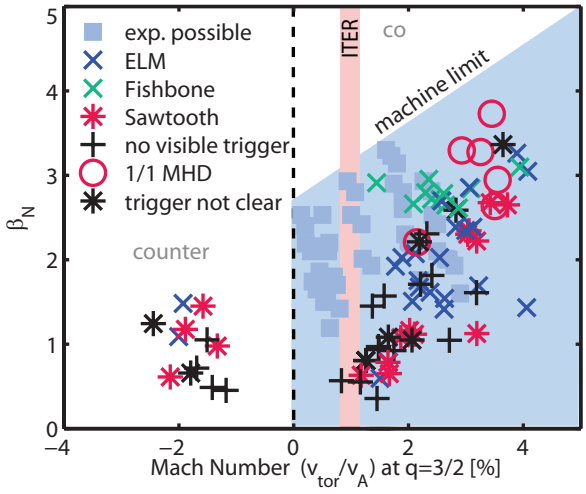

Figure 3. Normalised β_N at the onset of (3,2) NTMs versus the toroidal rotation velocity normalised to the Alfvén velocity at the resonant surface. The symbols indicate the different trigger mechanisms. The machine limit, indicating the experimentally achievable data range is also shown. The blueish grey boxes indicate the experimentally possible data range.

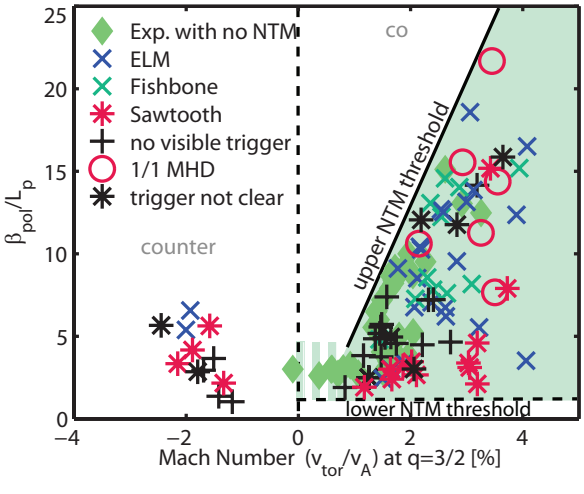

Figure 4. (3,2) NTM onset threshold versus the toroidal rotation velocity divided by the Alfvén velocity at the resonant surface. The symbols indicate the different trigger mechanisms. Additionally, data points from time points without NTMs are shown as green diamonds.

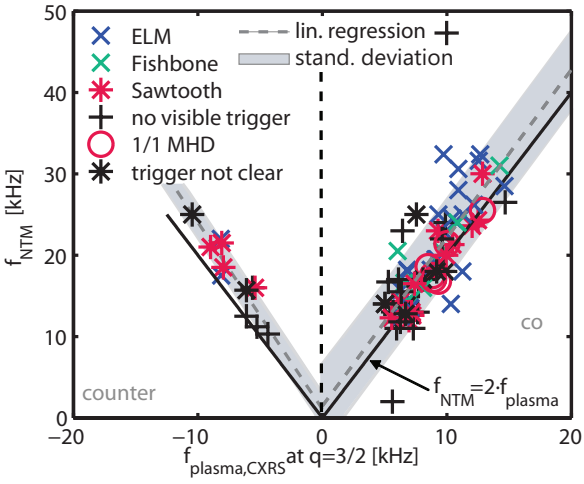

Figure 5. Comparison of the plasma toroidal rotation frequency at the q=3/2 surface measured with CXRS at the onset of the NTMs and the frequency of the NTM at the onset. A linear regression fit (dashed line), the standard deviation (grey shaded area) and the relation $f_{\mathrm{NTM}} = 2. \times f_{\mathrm{plasma,CXRS}}$ (straight line) are also indicated

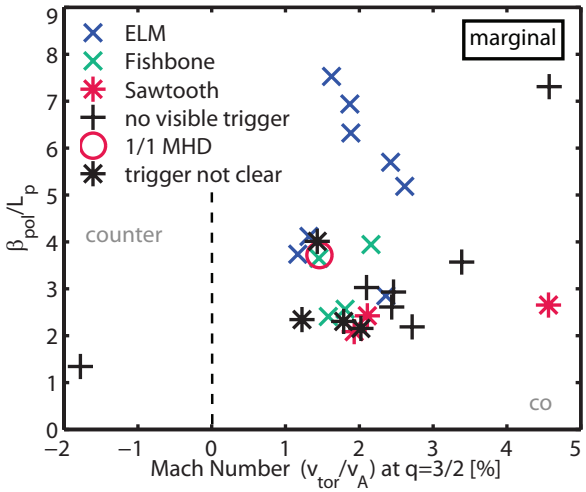

Figure 6. (3,2) NTM threshold at the marginal point versus the toroidal rotation velocity divided by the Alfvén velocity at the resonant surface. The symbols indicate the different trigger mechanisms.

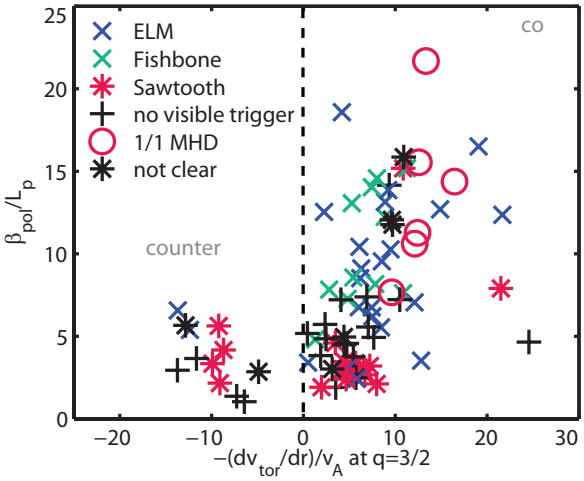

Figure 7. (3,2) NTM onset threshold versus the toroidal rotation gradient normalised to the Alfvén velocity at the resonant surface.

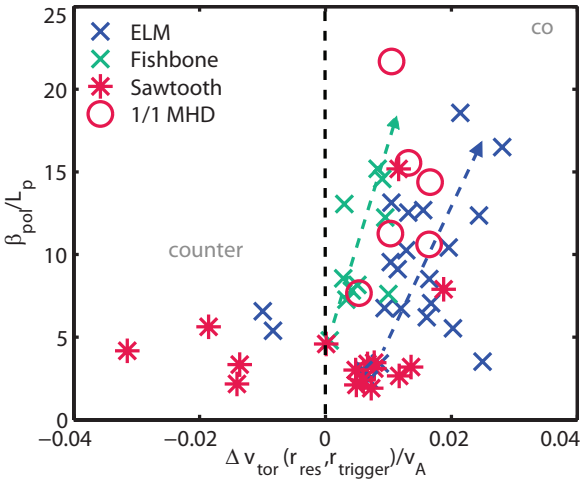

Figure 8. (3,2) NTM onset threshold versus the differential rotation between the trigger surface (either pedestal top for ELMs or q=1 surface for fishbones, sawtooth or other 1/1 activity) and island surface normalised to the Alfvén velocity.

[1] LA HAYE, R. J., BRENNAN, D. P., BUTTERY, R. J., and GERHARDT, S. P., Physics of Plasmas **17** (2010) 056110.
[2] WAELBROECK, F. L., CONNOR, J. W., and WILSON, H. R., Phys. Rev. Lett. **87** (2001) 215003.
[3] WILSON, H. R., ALEXANDER, M., CONNOR, J. W., et al., Plasma Physics and Controlled Fusion **38** (1996) A149.
[4] NAVE, M. F. F., KOSLOWSKI, H. R., CODA, S., et al., Physics of Plasmas **13** (2006) 014503.
[5] GRAVES, J. P., ANGIONI, C., BUDNY, R. V., et al., Plasma Physics and Controlled Fusion **47** (2005) B121.
[6] HEGNA, C. C., CALLEN, J. D., and LA HAYE, R. J., Physics of Plasmas **6** (1999) 130.
[7] BUTTERY, R. J., LA HAYE, R. J., GOHIL, P., et al., Physics of Plasmas **15** (2008) 056115.
[8] GERHARDT, S., BRENNAN, D., BUTTERY, R., et al., Nuclear Fusion **49** (2009) 032003.
[9] BUTTERY, R. J., GERHARDT, S., ISAYAMA, A., et al., Proceedings of the 22nd IAEA Fusion Energy Conference, Geneva, Switzerland, 2008 (International Atomic Energy Agency, Vienna, 2003), Paper No. IT/P6-8.
[10] RUTHERFORD, P. H., Physics of Fluids **16** (1973) 1903.
[11] SAUTER, O., LA HAYE, R. J., CHANG, Z., et al., Physics of Plasmas **4** (1997) 1654.
[12] QU, W. X. and CALLEN, J. D., (1985), University of Wisconsin Report No. UWPR 85-5.
[13] CARRERA, R., HAZELTINE, R. D., and KOTSCHENREUTHER, M., Physics of Fluids **29** (1986) 899.
[14] LA HAYE, R. J., Physics of Plasmas **13** (2006) 055501.
[15] SAUTER, O., ANGIONI, C., and LIN-LIU, Y. R., Physics of Plasmas **6** (1999) 2834.
[16] FITZPATRICK, R., Physics of Plasmas **2** (1995) 825.
[17] POLI, E., PEETERS, A. G., BERGMANN, A., GÜNTER, S., and PINCHES, S. D., Phys. Rev. Lett. **88** (2002) 075001.
[18] WILSON, H. R., CONNOR, J. W., HASTIE, R. J., and HEGNA, C. C., Physics of Plasmas **3** (1996) 248.
[19] BERGMANN, A., POLI, E., and PEETERS, A. G., Physics of Plasmas **12** (2005) 072501.
[20] GLASSER, A. H., GREENE, J. M., and JOHNSON, J. L., Physics of Fluids **18** (1975) 875.
[21] REICH, M., BOCK, A., MARASCHEK, M., and ASDEX Upgrade Team, Fusion Science and Technology **61** (2012) 309.
[22] VIEZZER, E., PüTTERICH, T., DUX, R., MCDERMOTT, R. M., and THE ASDEX UPGRADE TEAM, Review of Scientific Instruments **83** (2012) 103501.
[23] LA HAYE, R., PETTY, C. C., STRAIT, E. J., WAELBROECK, F. L., and WILSON, H. R., Physics of Plasmas **10** (2003) 3644.